# INTEGRATED GEOSCIENCES PROSPECTING FOR GOLD MINERALIZATION IN KWAKUTI, NORTHERN NIGERIA

**Ejepu, S. J.*, Olasehinde, P. I., Unuevho, C. I., Ako, T. A., Bassagi, M. and Abdullahi, D. S.**
Department of Geology, School of Physical Sciences, Federal University of Technology, Minna, Niger State, Nigeria.
*Corresponding Author: ejepu.jude@futminna.edu.ng. Tel: +2348034065079

**Abstract**
Geoscience prospecting for gold mineralisation was conducted in Kwakuti town located within Latitudes 9.362500°N to 9.387500ºN and Longitudes 6.920833ºE to 6.945833°E in northern Nigeria. The deployed geosciences techniques comprise surface geological mapping, analysis of SRTM DEM using *ArcGIS* software, processing and analysis of aeromagnetic total magnetic field intensity data using *Oasis Montaj* software and X-ray fluorescence analysis of soil samples. Migmatites and gneiss dominate the rock outcrops in the area. The migmatites occupy high elevations on the north-eastern and eastern portion of the area, where they display low magnetic field intensity values. The schist occupies moderate to low elevation areas and they display high magnetic field intensity values. The migmatites are dotted with quartz veins which constitute the gold mineralisation zone. Oval shaped high magnetic anomalous zones within the schist indicate basic intrusive into the schist. First derivative map of the magnetic field intensity data reveal NE-SW trending lineaments. They likely conducted hydrothermal fluids from the basic intrusive into the migmatites on the northeast, where gold mineralisation occurred by metasomatic ionic exchange. Spatial concentration of $TiO_2$ and $MnO_2$ are highest within the oval shaped high magnetic anomalous zones in the southern portion of the study area. This strengthens the inference that basic intrusive underlie the area. Gold concentration distribution pattern in the area is skewed NE-SW, thereby suggesting that the NE-SW structures control the mineralisation. Mining activities will be more efficient if directed along the NE-SW structural trend.
Keywords: Aeromagnetic data, Aero-radiometric data, Geologic mapping, Gold mineralisation, SRTM DEM, X-ray fluorescence.

## 1. Introduction

Lithologic units, lithologic boundaries, fractures and mineral accumulations are more accurately identified and delineated using the combination of surface geological mapping, remotely sensed radar data, geophysical data, and geochemical data on subsurface samples.

Aeromagnetic geophysical prospecting employs high magnetic susceptibility contrast between basement rocks to identify and map different lithologic units, geological structures and mineral accumulations within basement terrains (Kearey *et al*., 2002, Osinowo *et al.,* 2013).

The introduction of several computer software and improved digital mechanisms for data acquisition has expanded the scope of aeromagnetic applications. The combination of surface geological mapping, remotely sensed radar data, geophysical data, and geochemical data on subsurface samples were analysed using *Oasis Montage* to delineate different lithologic units, structures and gold mineralisation within part of Sheet 185NW Paiko (1: 50,000).

## 2.0 Location, geomorphological and geological setting of the area

The study area lies within Latitudes 9.362500°N to 9.387500ºN and Longitudes 6.920833ºE to 6.945833°E of Paiko Sheet 185NE (1: 50,000 Paiko). The tenement is located in Kwakuti community (Paikoro Local Government area of Niger State), a few kilometres off Suleja - Minna express way.

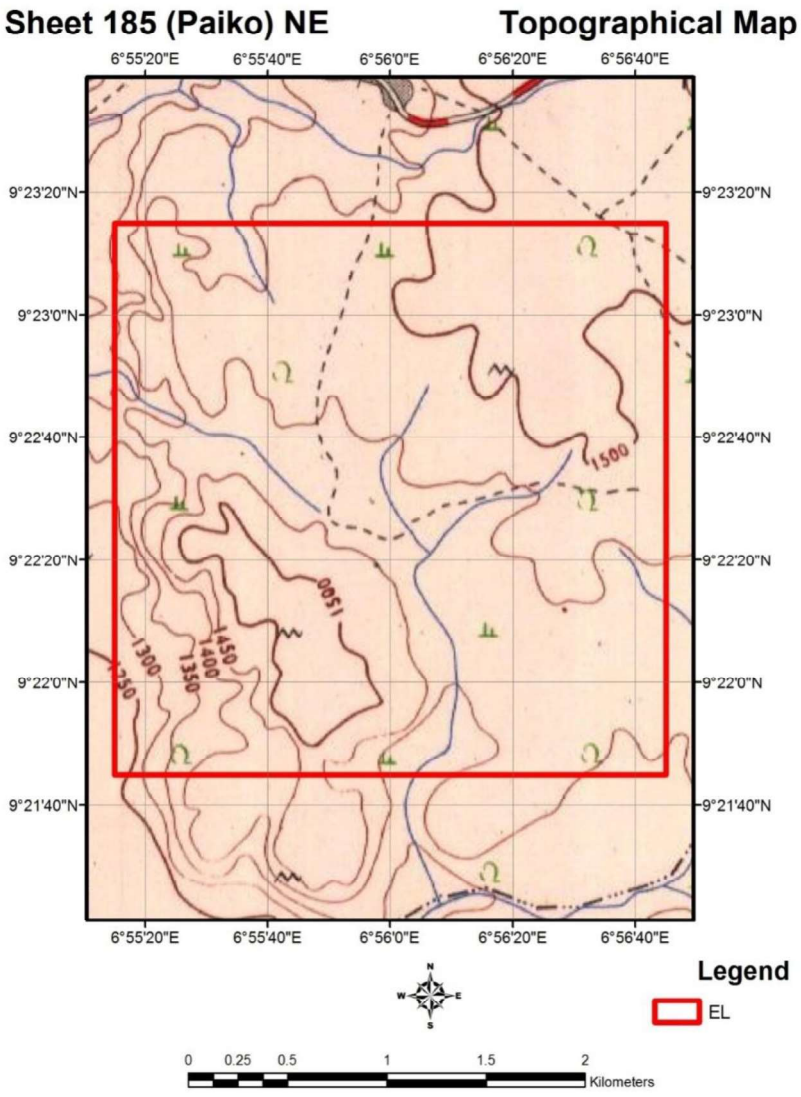


**Figure 1: Topographic map showing boundary Layout of the study area**

The area is characterized generally by undulating geomorphology. There are zones of low flat terrain that are dotted with a few hills, and display structurally controlled drainage of trellis pattern.

The area is an integral part of schist belt that hosts gold mineralization in Nigeria. The dominant rocks are the migmatites and schist. Pegmatite dykes occur within the schist while the migmatites outcrop over larger surface area than the schist. Feldspar, quartz and muscovite are major constituents within the schist. All the outcropping lithologic units in the area are transverse by quartz veins. The area is highly mineralized with gold occurring within pegmatite schist, quartz veins and in alluvium.

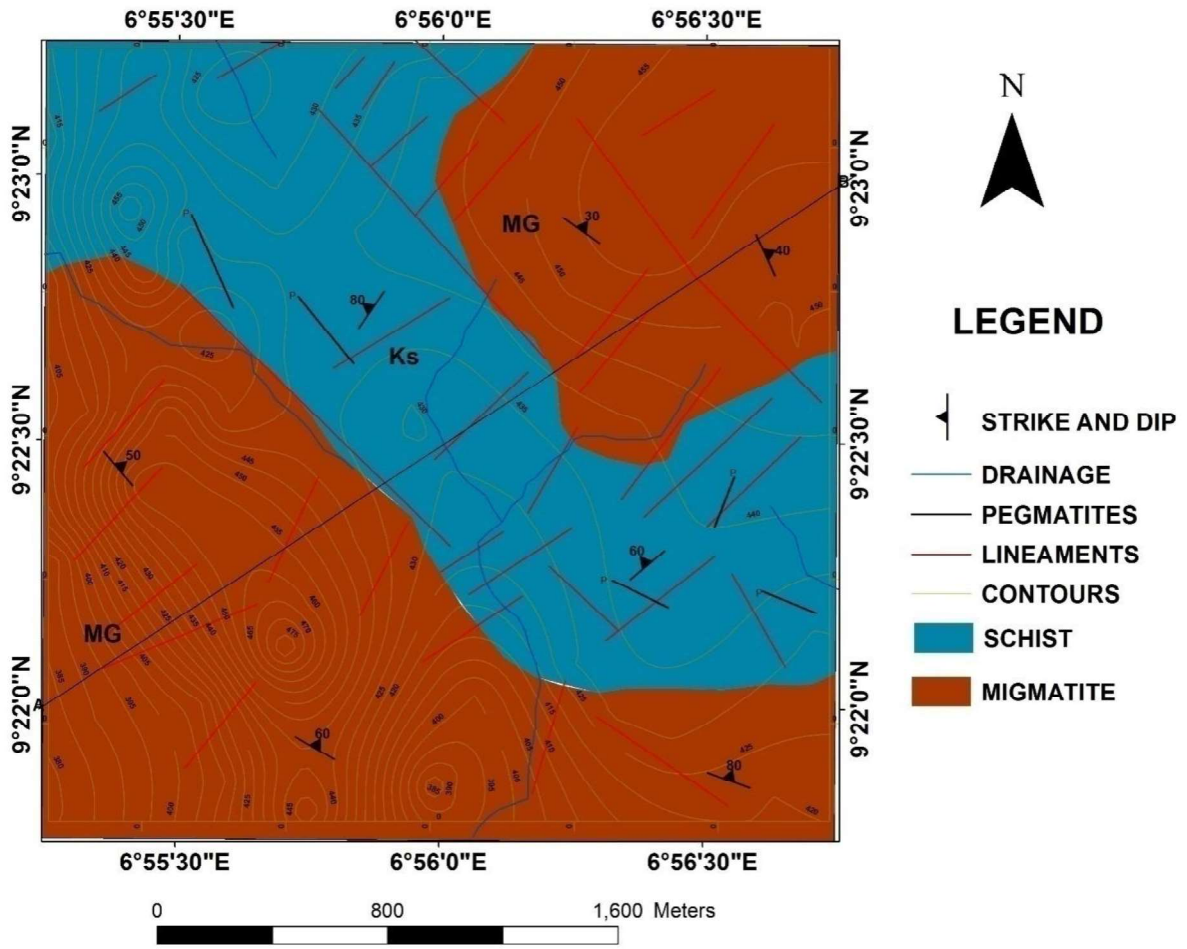


**Figure 2: Geologic map of the study area. Some fault lines are digitized from published geologic map. (Source: Nigerian Geological Survey Agency (NGSA), 2009).**

The structural elements in the study area include joints, faults, foliations and minor folds. The migmatites and schist generally trend NE-SW. The quartz veins are found trending NE-SW and in some areas. The quartz veins are seen be of great importance in our study because they host there are cases of gold infillings within them. Most of these structural elements do not appear on the map due to the scale of the map. Dolerite dykes are seen cutting across some of the outcrops. Fracturing may be as a result of thermo tectonic deformational events mostly of the Eburnean and Pan-African Orogeny (Oluyide, 1988). The dominant NE-SW structural trend coheres with the tectonic grain of the schist belt (Olasehinde *et al.,* 2013; Ejepu et al., 2015).

## 3.0 Methodology

Primary mineralization in Nigeria are mostly lithologically and structurally controlled (Ajakaiye *et al*., 1991). Structures include faults, shear zones (lineaments), pegmatites, quartz and quartzite veins. The methodology for this study was therefore structured to capture the general trends of surface and subsurface structures which control primary gold mineralization in the area. The exercise comprised surface geological mapping, lithologic and structural analysis of remote sensing images, pitting and sample collection. Soil samples were collected in the neighbourhood of stream channels and analysed using X-ray fluorescence.

### 3.1 Geologic mapping

Geological mapping exercise was carried out by locating areas of good outcrop exposures. Mapping was done using a topographic map on a scale of 12,500. Areas of geological interest were studied and tracked with the aid of a GPS device. Captured spatial data were tied to UTM, WGS 84 Zone 32N system. Data collected from the field were downloaded into the computer and developed into useful information with ArcGIS software. The success of the remote sensing and geological studies conducted on the area led to delineating regions with

high geological confidence of gold deposit occurrence. Faults and joints were investigated and strike and dip and of the fracture set were recorded using compass clinometers. Ground-truthing was also done on information extracted from remote sensing.

### 3.2 Aeromagnetic data processing and interpretation

The aeromagnetic data was obtained from NGSA. The data was acquired along a series of NE-SW tie lines direction with a flight line spacing of 500 m and terrain clearance of 80 m. The average magnetic inclination and declination across the survey is -5.49° and -1.99°, respectively. The data was gridded using the minimum curvature gridding method (Briggs, 1974). The micro-leveled magnetic data covering the study area was windowed out using the vertices coordinates in Oasis Montaj software. The total magnetic intensity field has been IGRF (International Geomagnetic Reference Field, 2009) corrected and super-regional field of 32000nT was deducted from the raw data. The airborne magnetic data were processed in *Oasis montaj* software, while information extraction and interpretation was done using *ArcGIS* software. The magnetic data was initially subjected to Reduction to the Magnetic Equator (RTE) and was further processed to investigate the presence of buried structures that might be relevant in the mineral exploration study. Directional and normalised derivatives were calculated to accentuate near surface structures from which lineaments were identified and delineated. These include First vertical, total horizontal and tilt derivatives, analytic signal. Source Parameter Imaging algorithm was applied to the RTE magnetic data to model depth to causative bodies.

#### 3.2.1 Reduction to Magnetic Equator (RTE)

Due to the inherent problem of low latitude anomaly shift, the magnetic grid was reduced to the equator and then inverted (Geosoft Inc., 2014). This was done with the aim of making magnetic anomalies to centre on their respective causative bodies.

#### 3.2.2 First Vertical Derivative (1VD)

MAGMAP was used to calculate the first vertical derivative of the magnetic data. This enhancement sharpens up anomalies over bodies and tends to reduce anomaly complexity, allowing a clearer imaging of the causative structures (Geosoft Inc., 2014). The transformation can be noisy since it will amplify short wavelength noise.

#### 3.2.3 Total Horizontal Derivative and Tilt Derivative

The Total Horizontal Derivative and the tilt derivative are both useful in mapping shallow to near surface basement structures (Geosoft Inc., 2014). These enhancements are also designed to image faults and contact features. They complement the results of the vertical derivative processing.

#### 3.2.4 Analytic Signal

The analytic signal processing generates a maximum directly over discrete magnetic bodies, as well as over their edges. The width of a maximum, or ridge, is an indicator of the depth to the contact. This transformation is often useful at low magnetic latitudes because of the inherent problems with RTP at such low latitudes (Geosoft Inc., 2014).

### 3.3 Radiometric data processing and interpretation

Airborne gamma-ray data are used as an aid to lithological mapping. Often, there is a good correlation between patterns in the radiometric data and unweathered rocks (Milligan & Gunn, 1997). This information complements magnetic, electromagnetic and geochemical data normally acquired during mineral exploration programs. This technique is cost-effective and rapid for geochemical mapping of the radioactive elements such as potassium, uranium and thorium. Radiometric surveys detect and map natural radioactive emanations, called gamma rays, from rocks and soils. Gamma-ray spectrometry (GRS) can be very helpful in mapping surface geology. The method provides estimates of apparent surface concentrations of the most common naturally occurring radioactive elements comprising potassium (K), equivalent uranium (eU), and equivalent thorium (eTh). The use of the method for geological mapping is based on the assumption that absolute and relative concentrations of these radio elements vary measurably and significantly with lithology.

### 3.4 Pitting

Locations for pitting were chosen from analysis of aeromagnetic map. Seven pits were dug to ascertain spatial extent of subsurface mineral occurrence. This is aimed at delineating or establishing a target size which is an area which is more mineralized.

### 3.5 Geochemical analysis

Stream sediments were collected based on the anomalous regions from the geophysical surveys. The site for the sampling coincided in drainage channels and samples were taken at about 0.3 m from the surface the stream. The samples were put in a plastic bag and then properly labelled and sent to the laboratory for analysis. X-ray fluorescence was performed on the samples for both major oxides and trace elements. Samples were prepared using pulverisation and palletisation methods. The selection of filters was guided by a given periodic table used for elemental analysis. Time of measurement for each sample was 100 seconds and the medium used was air throughout.

## 4.0 Results

### 4.1 Field investigations

Figure 2 is a digital elevation model of the study area. It reveals high elevation regions on the north-eastern and eastern portions of the area. Low elevation regions dominate the south-western and western portions.

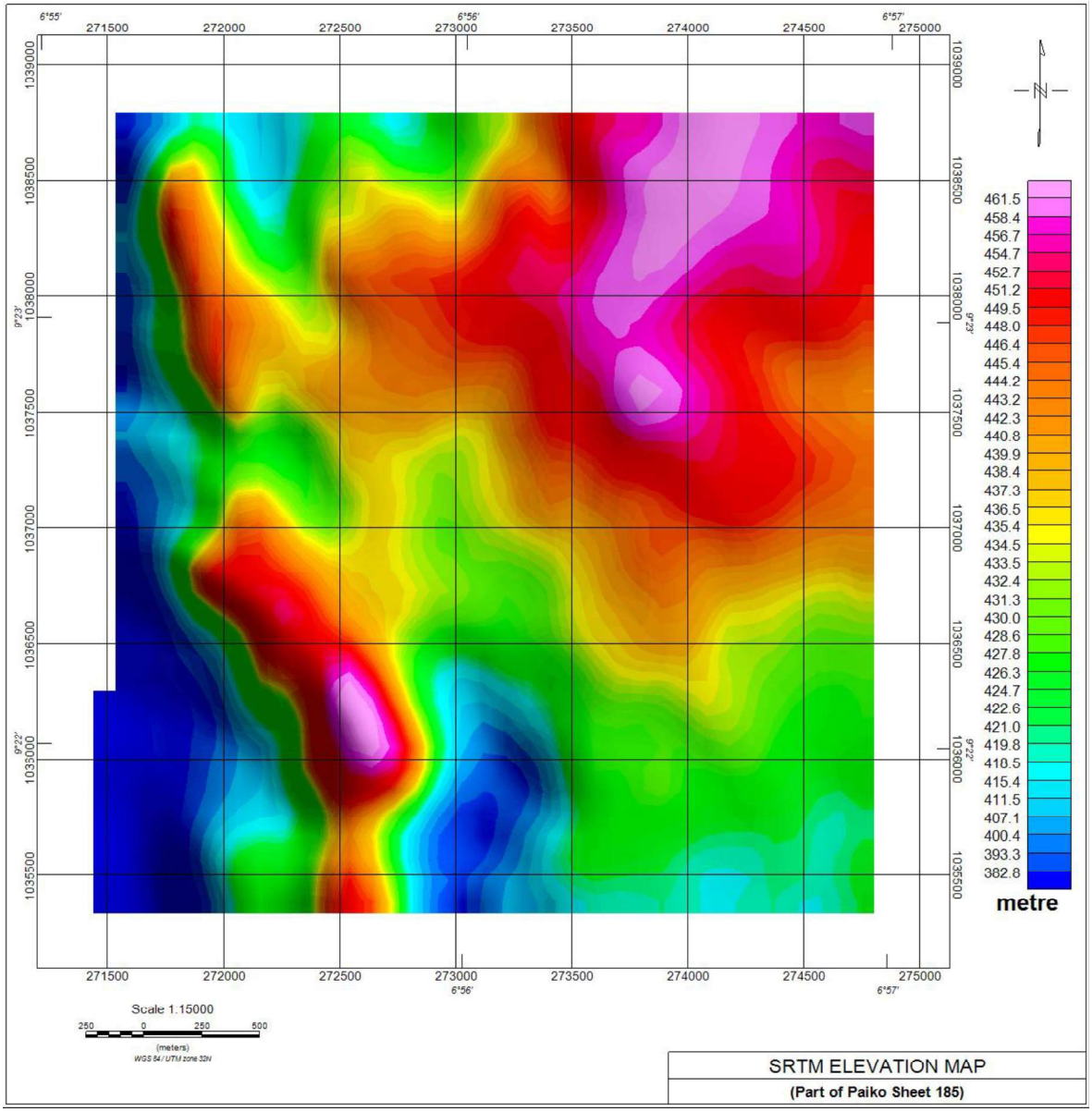


**Figure 3: SRTM elevation map.**

## 4.2 Geophysical data processing and interpretation

Figure 4 is the reduced to Equator (RTE) map generated from the total intensity magnetic anomaly (TIMA) data for the study area. The blocked region is the region covered by SRTM elevation map of figure 3. The map reveals that magnetic field intensity values that range from 40 to 67nT characterise the rocks in the study area. The high elevations regions (Figure 3) coincide with very low magnetic regions (figure 4), and are underlain with migmatites and dykes. Areas of moderate elevation are associated with high magnetic anomaly corresponding to schistose rocks.

Contact zones recorded low magnetic anomaly. This is an indication of demagnetization of magnetite minerals to hematite minerals with low magnetic response as a result of hydrothermal fluid flow through fractures and faults (Wilford *et al,* 1997). This is as a result of severe shearing and faulting at the contact zones. This prospective fault-bounded contact between the schists and the migmatites may potentially hosts mineralization zones in the area.

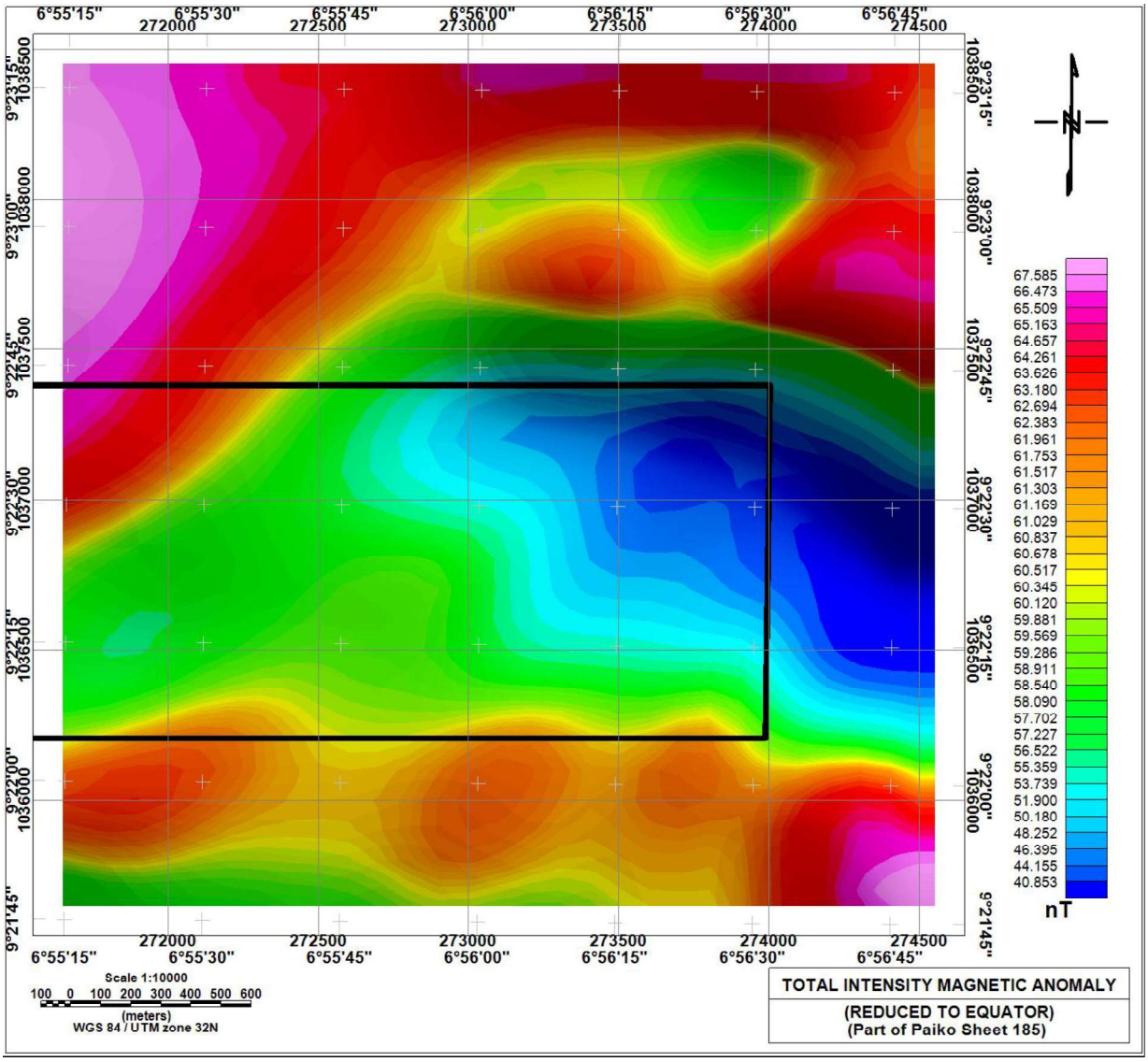


**Figure 4: Reduce-to-Equator total intensity magnetic anomaly map. Map was produced using Geosoft Oasis montaj. Black outline represents coverage where samples were taken for geochemical analysis.**

### 4.2.1 First Vertical Derivative (FVD)

The FVD map reveals NE-SW trending lineaments. Oval shaped anomalies with high total magnetic intensity values in the southern portion of figure 5 may indicate basic intrusives into the schist.
The quartz veins are hosted mainly in migmatites and are closely associated with the gold mineralization. The NE-SW trending lineaments are likely fractures that conducted hydrothermal fluids from basic intrusive into migmatites on the northeast.

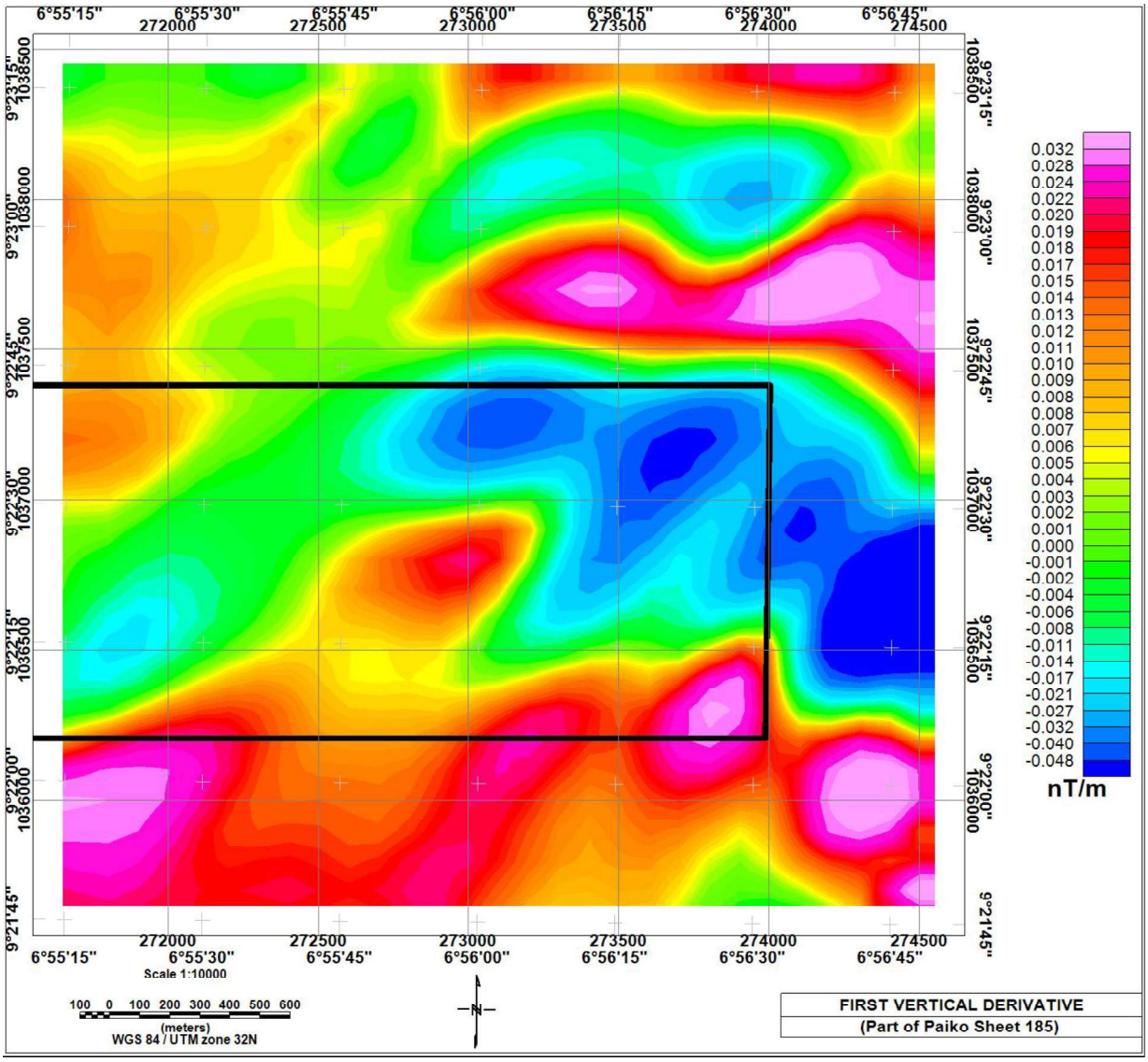


**Figure 5: First vertical derivative (FVD) map. Map was produced using Geosoft Oasis montaj. Black outline represents coverage where samples were taken for geochemical analysis.**

### 4.2.2 Tilt Derivative map (TDR)

The NE-SW trending lineaments are also revealed in the TDR map (figure 6). The map also reveals NW-SE trending lineaments on its north-eastern portion. Both lineaments constitute a conjugate fracture system. Since the NE-SW trending lineaments run through the schist and migmatites, they seem to control the mineralisation in the area.

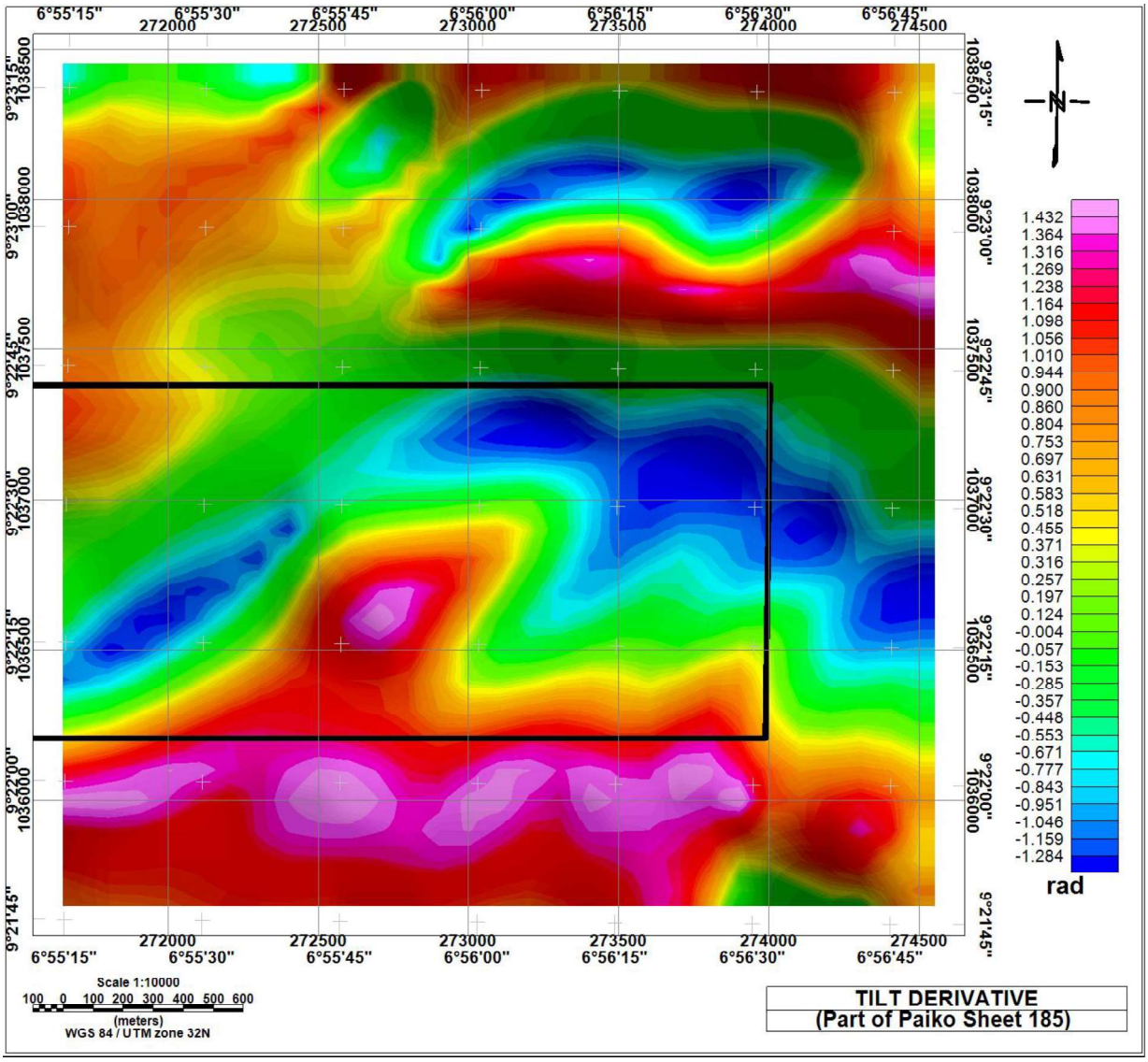


**Figure 6: Tilt Derivative map. Map was produced using Geosoft Oasis montaj. Black outline represents coverage where samples were taken for geochemical analysis.**

### 4.2.3 Analytic Signal (AS)

The NW-SE trending lineaments are indicated on the AS map (figure 7). It also revealed high magnetic anomaly zones in the north-eastern portion. The lineaments and the high magnetic anomaly

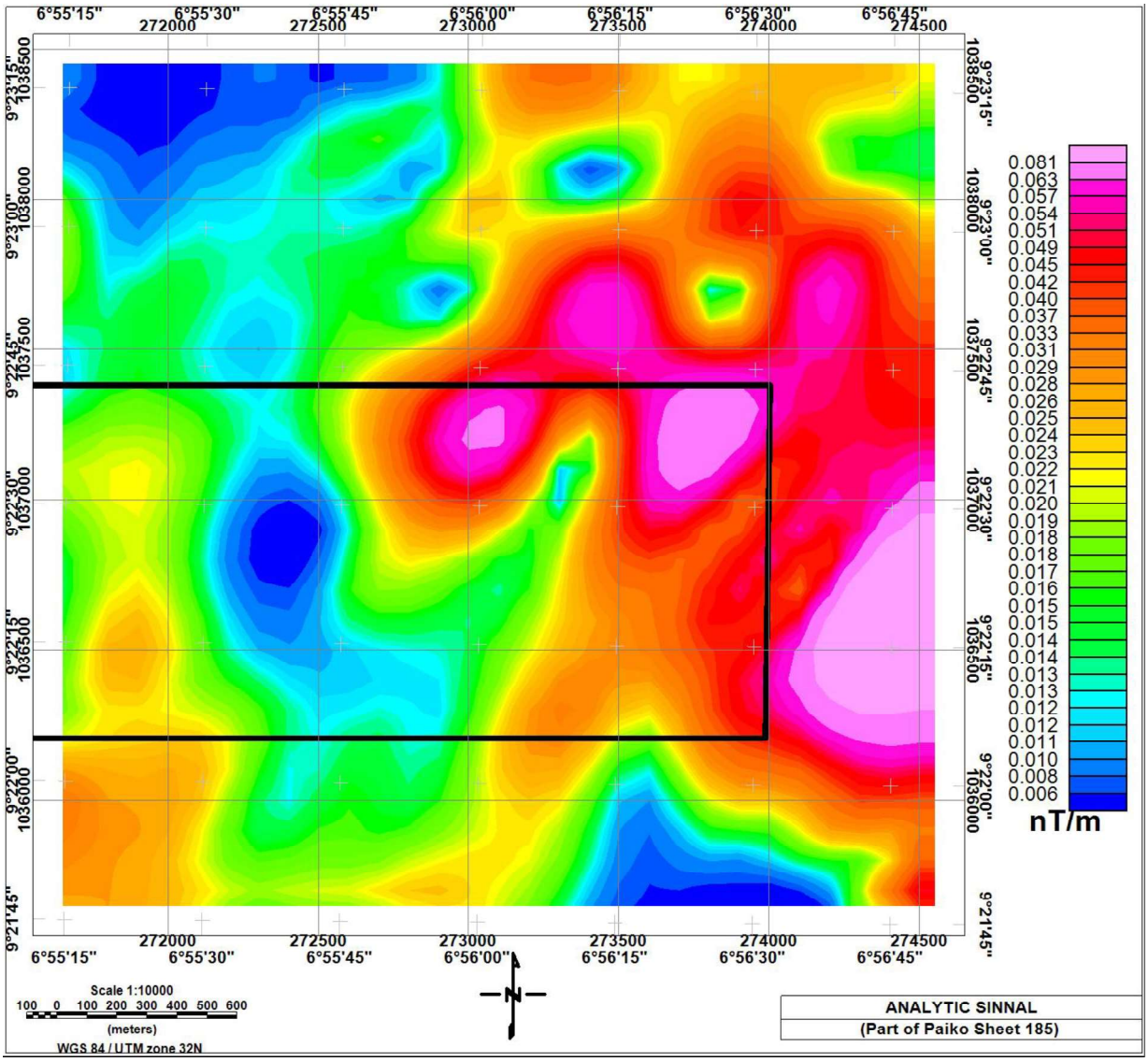


**Figure 7: Analytic signal map. Map was produced using Geosoft Oasis montaj. Black outline represents coverage where samples were taken for geochemical analysis.**

Figure 8 is a map showing the composite lineaments obtained from the different processing of the total magnetic field intensity data, and the lineaments determined from surface geological mapping exercise. The dominant lineaments are the conjugate NW-SE and NE-SW fractures.

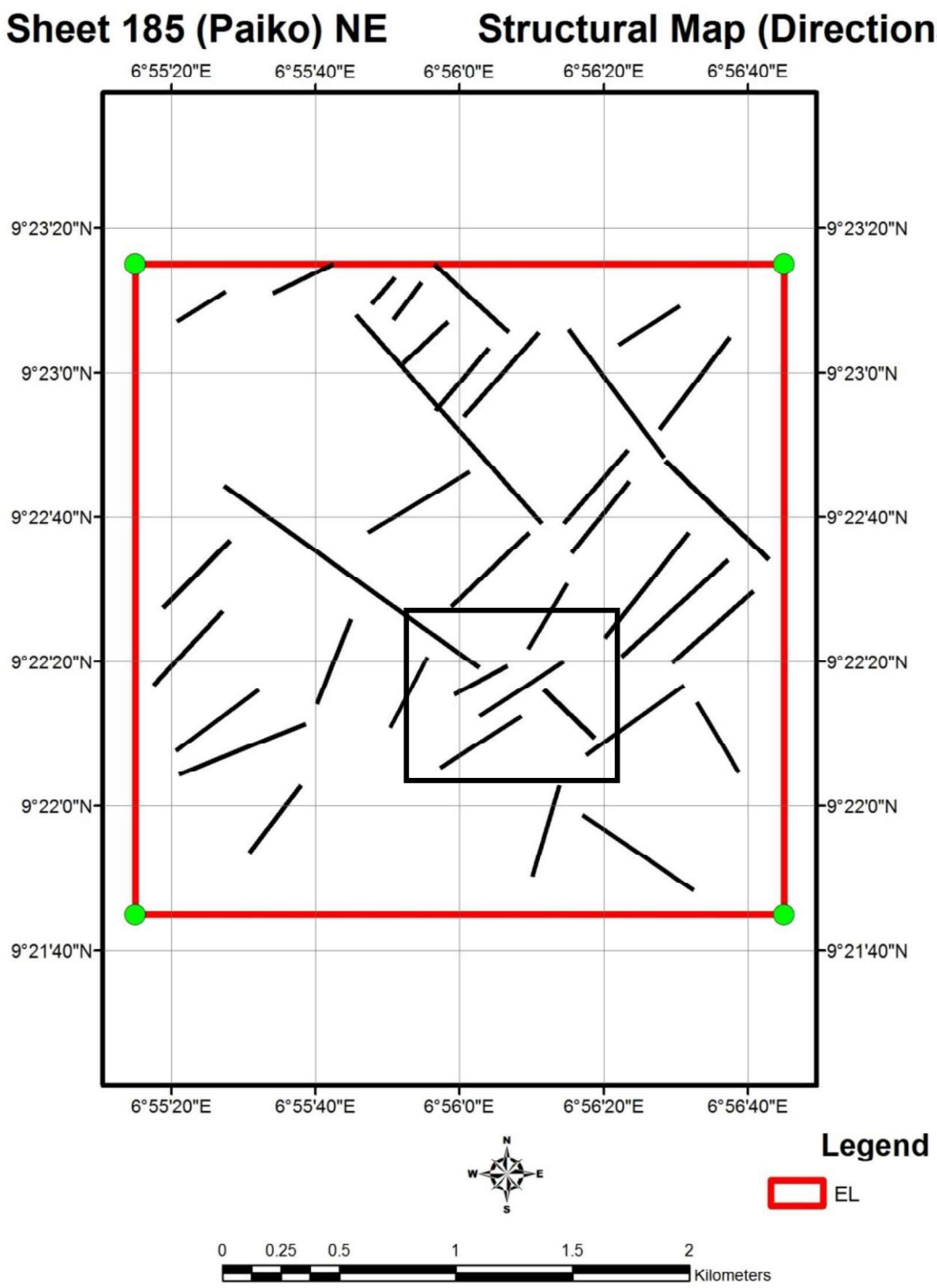


**Figure 8: Lineament map of the study area. Some mapped surface structures are also represented.**

### 4.3 Ternary Image

The ternary image (**Figure 9**) comprises of colours generated from the relative intensities of the three components and represents subtle variations in the ratios of the three bands with K assigned to red, U to blue and Th to green. The composite image presents strong spatial correlations with the known geologic units and the most prominent features in the K, Th, and U images. The most notable units in the ternary image are the mafic and magnetite rich migmatite formations which are represented in cyan and also notable in both U and

Th maps. In addition, the migmatite with high K concentration and some traces of U are given a magenta colour. This strong correlation is based on the fact that the migmatite are made up of the potash-rich (high K concentration) regolith which come in the form of muscovite and biotite as well as the mineral constituents of the pegmatite dykes (Wilford et al, 1997).

The K, Th and U map show that the schist recorded weak anomaly of K and Th but strong U anomaly. A long denudation period of weathering has probably depleted most of the U concentration of migmatites within the western portion of the ternary map. The dark regions which occur within faulted zones and in some areas at the contact zones of the rock formation can be attributed to the low concentration of the K, Th and U. The light yellow zones in the ternary image are indications of high concentration of K, Th but low U concentrations.

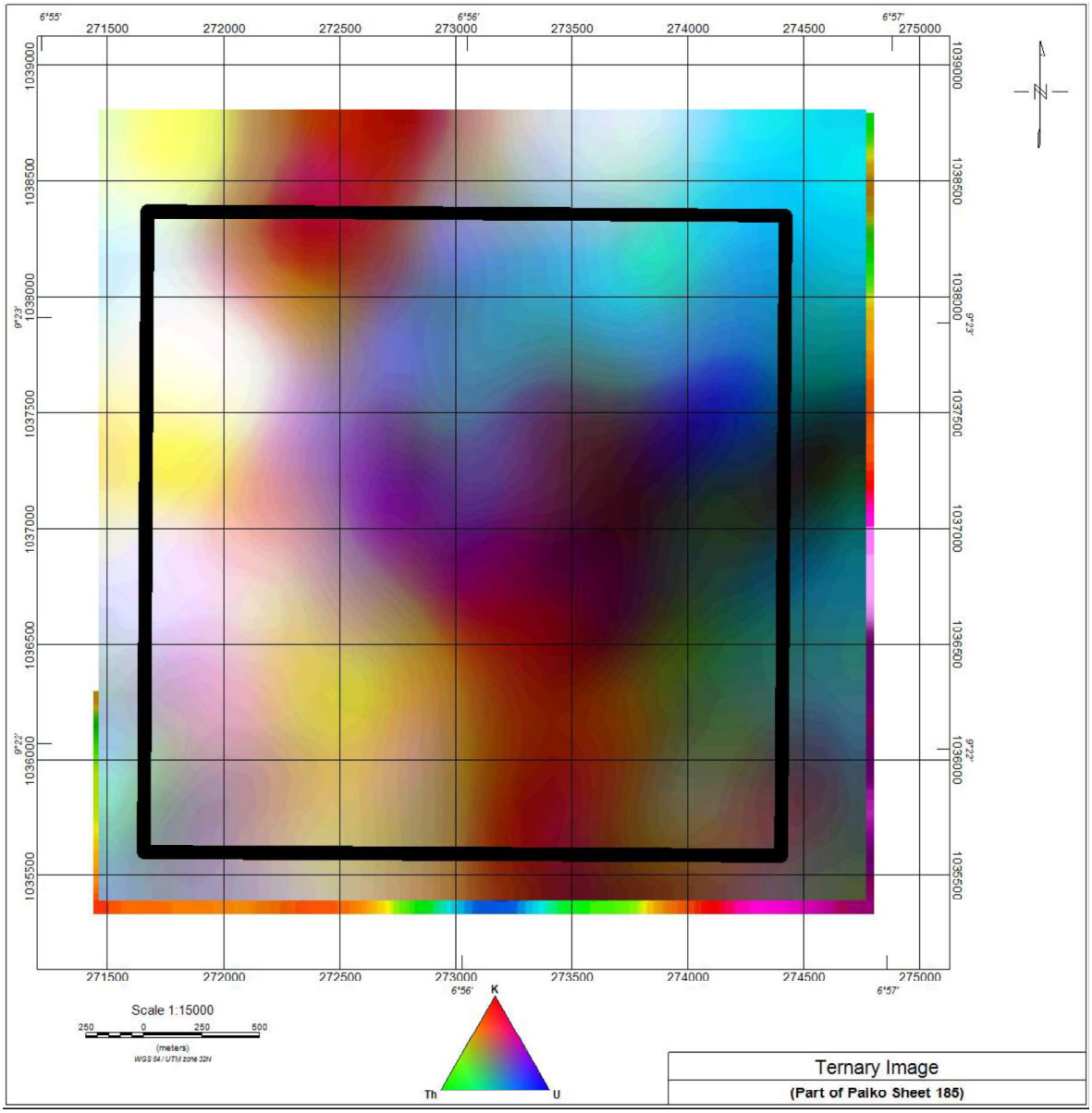


**Figure 9: Ternary Image Map produced from equivalent potassium, thorium and uranium concentrations. Map was produced using Geosoft Oasis montaj.**

### 4.4 Pitting and geochemical analyses

The geographic coordinates of the sampled pits are presented as table 1.

**Table 1: Geographic coordinates of the pits.**

| PIT NUMBER | LONGITUDE (E) | LATITUDE (N) |
|---|---|---|
| 01 | 6°56′03.0″ | 9°22′05.3″ |
| 02 | 6°55′23.7″ | 9°22′11.9″ |
| 03 | 6°55′09.3″ | 9°22′24.4″ |
| 04 | 6°55′16.8″ | 9°22′33.4″ |
| 05 | 6°55′26.3″ | 9°22′40.4″ |
| 06 | 6°55′34.9″ | 9°22′37.2″ |
| 07 | 6°56′31.6″ | 9°22′43.3″ |

The concentration of the major oxides in percentage is given in table 2

**Table 2: Major oxides (%)**

The determined trace elements and rare earth elements are shown in table 3.

| SAMPLE ID | SiO2 (%) | Al2O3 (%) | SO3 (%) | P2O5 (%) | Na2O (%) | K2O (%) | CaO (%) | MgO (%) | TiO2 (%) | Fe2O3 (%) | MnO (%) | $H_2O^+$ (%) |
|---|---|---|---|---|---|---|---|---|---|---|---|---|
| **LOC. 1** | 54.20 | 14.08 | - | - | 1.04 | 8.26 | 1.20 | 0.24 | 4.83 | 10.40 | 0.06 | 5.68 |
| **LOC. 2** | 69.80 | 8.41 | - | - | 0.02 | 2.40 | 4.95 | 0.54 | 6.22 | 5.12 | 0.22 | 2.30 |
| **LOC. 3** | 48.10 | 19.00 | - | - | 0.41 | 4.24 | 0.78 | - | 1.86 | 18.10 | 0.16 | 7.33 |
| **LOC. 4** | 65.80 | 7.98 | - | - | 0.32 | 2.70 | 2.89 | 1.04 | 2.84 | 10.42 | 0.075 | 5.93 |
| **LOC. 5** | 59.70 | 18.00 | - | - | 1.02 | 5.51 | 0.47 | - | 2.55 | 7.99 | 0.035 | 4.72 |
| **LOC. 6** | 60.00 | 13.21 | - | - | 1.04 | 7.09 | 1.68 | 0.02 | 1.68 | 9.00 | 0.12 | 6.14 |
| **LOC. 7** | 56.20 | 18.34 | - | - | 1.54 | 5.34 | 1.90 | 0.03 | 3.03 | 8.84 | 0.14 | 4.60 |

**Table 3: Trace elements/Rare Earth metals (ppm)**

| ELEMENTS (ppm) | LOC. 1 | LOC. 2 | LOC. 3 | LOC.4 | LOC. 5 | LOC. 6 | LOC. 7 |
|---|---|---|---|---|---|---|---|
| **Ag** | 3.040 | 1.606 | 3.346 | 1.354 | 1.628 | 2.252 | 1.790 |
| **As** | 0.008 | <0.001 | 5.001 | <0.001 | 0.900 | <0.001 | <0.001 |
| **Au** | 2.940 | 0.872 | 3.588 | 2.018 | 2.620 | 0.296 | 1.954 |
| **Bi** | 1.240 | 2.140 | 1.483 | 3.025 | 3.312 | 0.895 | 0.864 |
| **Cd** | <0.001 | <0.001 | <0.001 | <0.001 | <0.001 | <0.001 | <0.001 |
| **Ce** | <0.001 | <0.001 | <0.001 | <0.001 | <0.001 | <0.001 | <0.001 |
| **Co** | <0.001 | <0.001 | <0.001 | <0.001 | <0.001 | <0.001 | <0.001 |
| **Cr** | 0.880 | 0.083 | 0.630 | 2.400 | 1.420 | 0.635 | 0.782 |
| **Cs** | <0.001 | <0.001 | <0.001 | <0.001 | <0.001 | <0.001 | <0.001 |
| **Cu** | 0.100 | 0.130 | 0.220 | 0.044 | 0.120 | 0.053 | 0.055 |
| **Eu** | 0.480 | 0.540 | 0.530 | 0.170 | 0.200 | 0.230 | 0.420 |
| **Ga** | 0.010 | <0.001 | 4.001 | <0.001 | <0.001 | 0.801 | <0.001 |
| **Ge** | <0.001 | <0.001 | <0.001 | <0.001 | <0.001 | <0.001 | <0.001 |
| **Mo** | <0.001 | <0.001 | <0.001 | <0.001 | <0.001 | <0.001 | <0.001 |
| **Nb** | <0.001 | <0.001 | <0.001 | <0.001 | <0.001 | <0.001 | <0.001 |
| **Ni** | <0.001 | <0.001 | <0.001 | <0.001 | <0.001 | <0.001 | <0.001 |
| **Os** | <0.001 | <0.001 | <0.001 | <0.001 | <0.001 | <0.001 | <0.001 |
| **Pb** | 0.180 | 0.084 | 10.087 | <0.001 | 0.690 | <0.001 | <0.001 |
| **Re** | 0.100 | 0.070 | 0.200 | 0.700 | 0.042 | 0.130 | 0.120 |
| **Sr** | 0.018 | 0.110 | 0.140 | 0.290 | <0.001 | 0.970 | 0.010 |
| **Ta** | <0.001 | <0.001 | <0.001 | <0.001 | <0.001 | <0.001 | <0.001 |
| **Th** | <0.001 | <0.001 | <0.001 | <0.001 | <0.001 | <0.001 | <0.001 |
| **Tl** | <0.001 | <0.001 | <0.001 | <0.001 | <0.001 | <0.001 | <0.001 |
| **U** | <0.001 | <0.001 | <0.001 | <0.001 | <0.001 | <0.001 | <0.001 |
| **V** | 0.702 | 0.512 | <0.001 | 0.680 | 0.730 | 0.850 | 0.500 |
| **W** | <0.001 | <0.001 | <0.001 | <0.001 | <0.001 | <0.001 | <0.001 |
| **Zn** | 0.840 | 1.470 | 0.180 | 2.000 | 1.700 | 0.370 | 1.002 |
| **Zr** | 48.00 | 25.000 | 6.500 | 1.200 | 1.770 | 0.288 | 0.2985 |

The spatial distribution of $TiO_2$, and $MnO_2$ are shown in figures 9 and 10 respectively. The highest concentration of these oxides is in the south-western portion of the area. This supports the interpretation that oval shaped high anomalies in the FVD map (figure 5) are basic intrusive. Figure 11 shows the spatial distribution of gold in the area. The NE-SW alignment of the concentration pattern supports the interpretation that the NE-SW fractures conducted hydrothermal fluids from basic intrusive in the SW to migmatites in the NE.

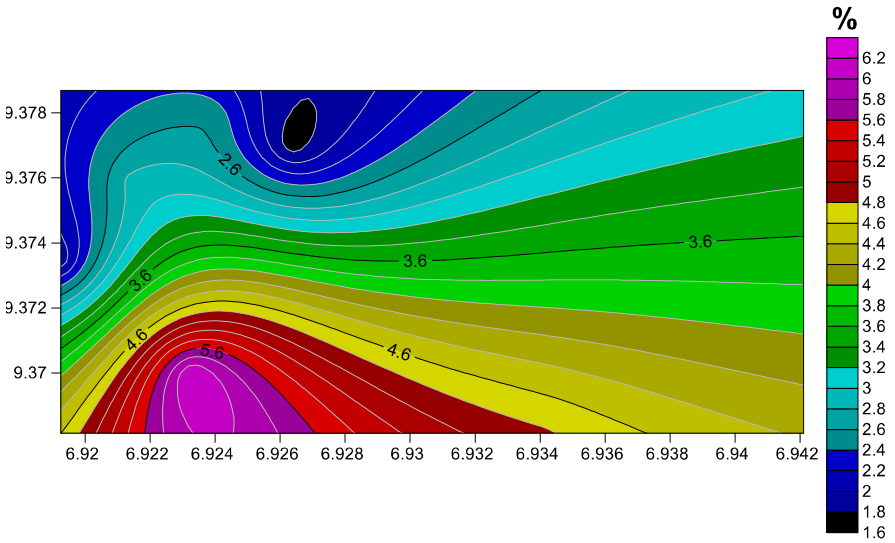


Figure 10: Contour plot of geochemical distribution of $TiO_2$ (in %) for Pit samples in the area.

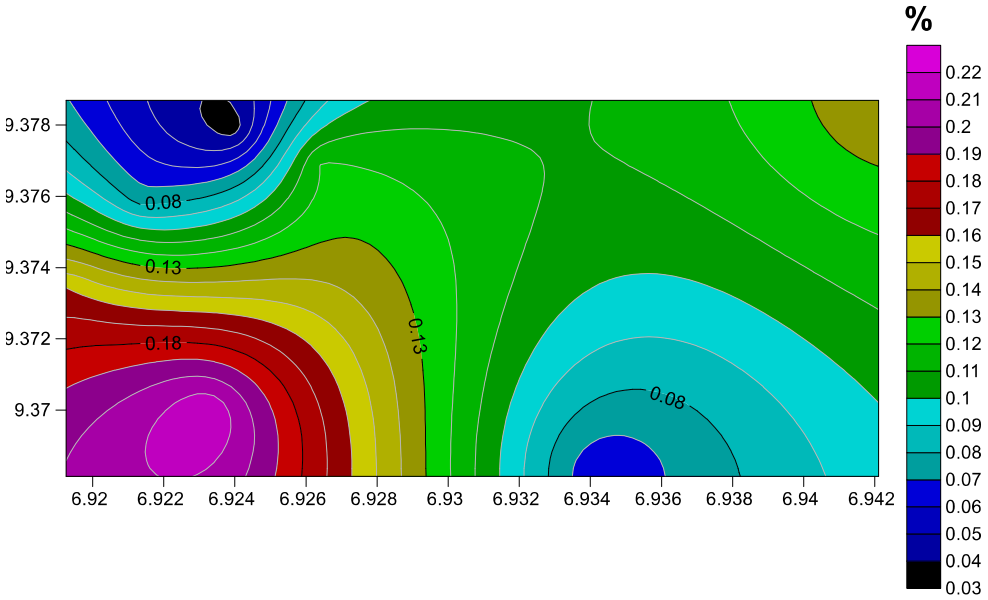


Figure 11: Contour plot of geochemical distribution of MnO (in %) for Pit samples in the area.

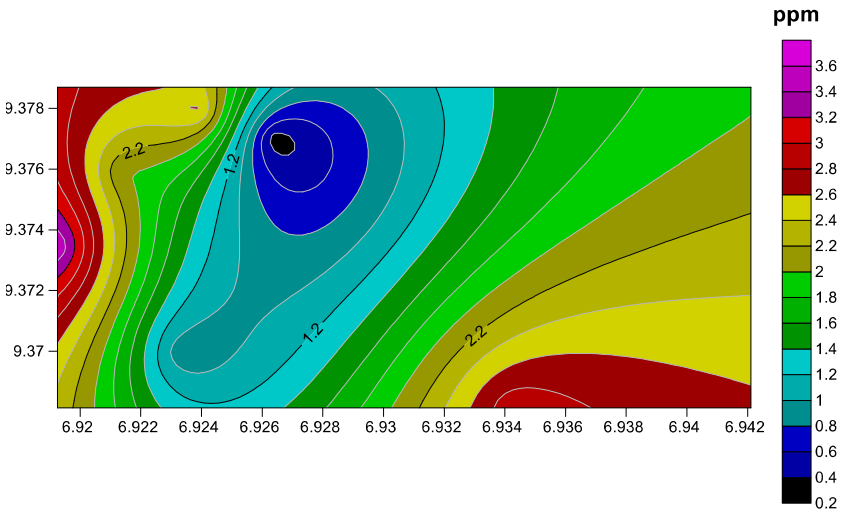


Figure 12: Contour plot of geochemical distribution of Au (ppm) for Pit samples in the area.

## 5.0 Conclusion and Recommendation

The area has undergone a pronounced tectonic activity resulting in shearing and fracturing. A common feature of the rare-metal pegmatites and veins in Nigeria is their close proximity to major and subsidiary fault structures. So, the sheared zone and fractures are potential channels for mineralization fluids. The observed zonation in the magnetic data and the potassic alteration in the ternary image are indication of hydrothermal alteration associated with mineralization. Often this alteration signature may be broad and laterally extensive providing a larger exploration target. The contacts between different geological units, the intersections between linear features, sheared and fractured zones are potential traps for minerals and therefore give a significant exploration vectors.

The locations of core drilling will be determined based on recommended sites from the detailed geophysical and geochemical form of exploration. The core samples should advisably be analysed in a world class laboratory in other to ascertain the grade.
It is recommended that fire assay geochemical analysis be performed on the soil samples that have been taken from various anomalous regions in the prospect area.

## References

Abedi, M. & Norouzi, G. H. (2012). Integration of various geophysical data with geological and geochemical data to determine additional drilling for copper exploration. *Journal of Applied Geophysics,* 83**,** 35-45.

Abedi, M., Gholami, A. & Norouzi, G. H. (2013). A stable downward continuation of airborne magnetic data: A case study for mineral prospectivity mapping in Central Iran. *Computers & Geosciences,* 52**,** 269-280.

Abu El-Ata, A. S., EI-Khafeef, A. A., Ghoneimi, A. E., AbdAlnabi, S. H. & Al-Badani, M. A. (2013). Applications of aeromagnetic data to detect the Basement Tectonics of Eastern Yemen region. *Egyptian Journal of Petroleum,* 22**,**277-292.

Ajakaiye, D. E., Hall, D. H., Ashiekaa, J. A., & Udensi, E. E. (1991). Magnetic anomalies in the Nigerian continental mass based on aeromagnetic surveys. *Tectonophysics*, 192(1), 211-230.

Briggs, I. C. (1974). Machine contouring using minimum curvature. *Geophysics*, *39*(1), 39-48.

Ejepu, S. J., Olasehinde, P. I., Omar D. M., Abdullahi, D. S, Adebowale, T. A., & Ochimana, A. (2015). Integration of Geology, Remote Sensing and Geographic Information System in assessing groundwater potential of Paiko Sheet 185 North-Central Nigeria. *Journal of Information, Education, Science and Technology*. 2(1), 145 – 155.

Geosoft (2014). GM-SYS Gravity & Magnetic Modelling Software, Users Guide, v.4.10, Northwest Geophysical Associates, Inc., P.O. Box 1063, Corvallis, Oregon 97339-1063 USA, 2006.

Hirdes, W., Senger, R., Adjei, J., Efa, E., Loh, G. and Tetty, A. (1993) Explanatory Notes for the Geological Map of Southwest Ghana 1: 100,000, Sheet Wiawso (0603d), Asafo (0603c), Kukuom (0603b), Goaso (0603a), Sunyani(0703d) and Berekum (0703c). Geologisches Jahrbuch Reine B, Band B 83, Hannover, 139 p.

Kearey, P., Brooks, M. & Hill, I. (2002). *An introduction to geophysical exploration*, John Wiley & Sons.

Keating, P. B. (1995) A simple Technique to Identify Magnetic Anomalies Due to Kimberlite Pipes. *Exploration and Mining Geology*, **4**, 121-125.

Milligan, P.R. and Gunn P.J. (1997) Enhancement and Presentation of Airborne Geophysical. *AGSO*, *Journal of Australian Geology and Geophysics*, **17**, 64-74.

Olasehinde P. I., Ejepu S. J. & Alabi A. A. (2013). Fracture Detection in a Hard Rock Terrain Using Radial Geoelectric Sounding Techniques. *Water Resources Journal* 23(1&2), 1-19.

Oluyide, P.O. (1988). Structural trends in the Nigerian Basement Complex. In: Precambrian Geology of Nigeria. *Geological Survey of Nigeria*, pp. 93 - 98.

Osinowo, O. O., Akanji, A. O. & Olayinka, A. I. (2013). Application of High Resolution Aeromagnetic Data for Basement Topography Mapping of Siluko and Environs, South-western Nigeria. *Journal of African Earth Sciences*.

Reynolds, R.L., Rosenbaum, J.G., Hudson, M.R. and Fishman, N.S. (1990) Rock Magnetism, the Distribution of Magnetic Minerals in the Earth's Crust and Aeromagnetic Anomalies. *US Geological Survey Bulletin*, **1924**, 24-45.

Wilford, J.R., Bierwirth, P.N. and Craig, M.A. (1997) Application of Airborne Gamma-Ray Spectrometry in Soil/Regolith Mapping and Applied Geomorphology. *AGSO*, *Journal of Australian Geology and Geophysics*, **17**, 201-216.